Switching Between Crystallization and Amorphous Agglomeration of Alkyl Thiol-Coated Gold Nanoparticles

Tihamér Geyer
Center for Bioinformatics, Saarland University, D–66041 Saarbrücken, Germany

Philip Born and Tobias Kraus*
Structure Formation Group, INM—Leibniz Institute for New Materials, D–66123 Saarbrücken, Germany
(Received 10 May 2012; published 17 September 2012)

Crystalline and amorphous materials composed of the same atoms exhibit strikingly different properties. Likewise, the behavior of materials composed of mesoscale particles depends on the arrangement of their constituent particles. Here, we demonstrate control over particle arrangement during agglomeration. We obtain disordered and ordered agglomerates of the same alkyl thiol-coated gold nanoparticles depending on temperature and solvent. We find that ordered agglomeration occurs exclusively above the melting temperature of the ligand shells. Many-particle simulations show that the contact mechanics of the ligand shells dominate the order-disorder transition: Purely spherical particle-particle interactions yield order, whereas localized ''stiction'' between the ligand shells leads to disorder. This indicates that the ''stickiness'' and the packing of the agglomerates can be switched by the state of the ligand shells. It suggests that contact mechanics govern ordering in a wide range of nanoparticles.

DOI: 10.1103/PhysRevLett.109.128302 PACS numbers: 82.70.Dd, 65.80.−g, 66.30.Pa, 68.35.Rh

Controlling the crystallization of particles in the nanometer size range has broad implications. In biology for example, the protist *Paramecium* crystallizes certain proteins and changes their crystallinity to rapidly release energy for defensive purposes [1]. In materials synthesis, monodispersed nanoparticles have been assembled into crystalline ''superlattices'' with properties that are different from the continuous bulk [2–4]. It is technologically important to know under which conditions such lattices form. If we could control whether particles assemble into crystalline or amorphous agglomerates, we could change the material properties that depend on order.

The agglomeration of sterically stabilized nanoparticles in unpolar solvents can be induced by cooling the dispersion below a critical temperature at which the packing of the ligand chains changes [5–7]. Cooling has been reported to induce an attractive glass transition in such suspensions [8] and to yield irregularly packed agglomerates. Agglomeration can also be induced by precipitation by incompatible solvents [9,10], which can yield regular superlattices [2,9]. The agglomeration of charge-stabilized nanoparticles in water does not exhibit such a dichotomy. Lin *et al.* observed that the interactions of destabilized, aqueous gold nanoparticles upon contact are so strong that reconfiguration is impossible and fractal agglomerates form [11].

Here, we report the switching between amorphous and crystalline agglomeration of monodisperse gold nanoparticles coated by alkyl thiol monolayers. We show that the order depends on the contact mechanics of the ligand shells, which we control via temperature. At low temperatures, the ligand shells impede the lateral motion that is necessary for the particles to reach crystalline configurations [12], and amorphous agglomerates form.

A synthesis route adapted from Zheng *et al.* [13] was used in this work to obtain gold nanoparticles coated either with dodecanethiol (to which we refer as ''C12'' in the following), hexadecanethiol (''C16''), and octadecanethiol (''C18''). Transmission electron microscopy (TEM) confirmed the uniform gold core of all particle-ligand systems. The average core radius for the three particle types used was 3.2 ± 0.3 nm. Dynamic light scattering (DLS) indicated slightly larger hydrodynamic radii, proving that the cores were covered by the alkyl thiols: 4.5 nm for the particles coated with dodecanethiol, 5.2 nm for hexadecanethiol, and 5.3 nm for octadecanethiol. DLS experiments also indicated that the suspensions were free of agglomerates at least at temperatures above 30 °C after filtering.

The interactions between such ligand-coated particles are described by the Flory-Huggins theory [14]. Attractions should increase for poor solvents and low temperatures. In good, unpolar solvents, we found that below a ligand-specific temperature T_p, the particles started to agglomerate and the mean hydrodynamic radii measured by DLS increased. This transition was fully reversible: an increase of the temperature above T_p led to dissociation of the agglomerates as indicated by a decrease in the mean hydrodynamic radii. Figure 1 shows a typical DLS experiment that we used to quantify the temperature-dependent agglomeration. The agglomeration temperature T_p increased with the chain length N_c of the alkyl thiols from $T_p \approx -15$ °C for C12 to ≈ 20 °C for C16 to ≈ 30 °C for C18 particles. For all three nanoparticle types, TEM indicated spherical,

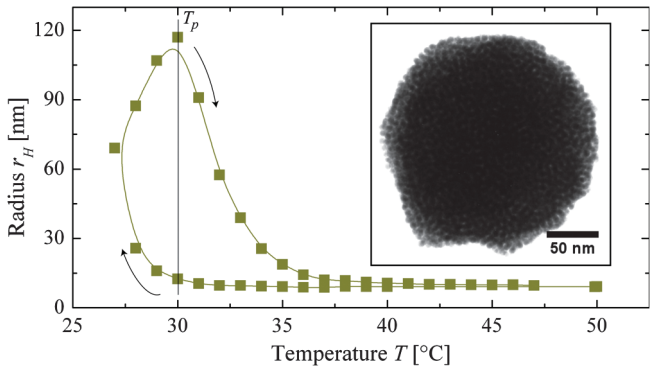

FIG. 1 (color). Mean hydrodynamic particle radii of C18 particles from DLS measurements as a function of temperature. At a ligand specific temperature T_p, the particles start to agglomerate upon cooling. Heating above this temperature dissolves the agglomerates reversibly. The inset shows a transmission electron micrograph of a typical spherical amorphous agglomerate formed upon cooling below T_p.

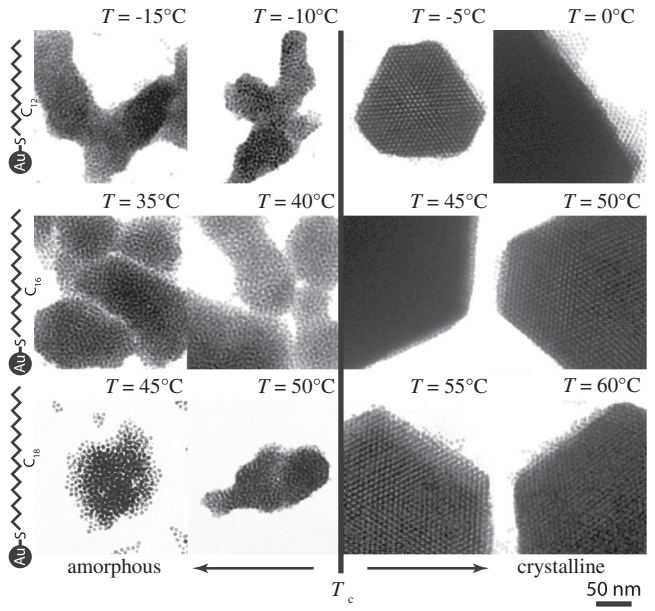

FIG. 2. Transmission electron micrographs of agglomerates formed upon addition of polar solvent at different temperatures. The ordering of the particles in the agglomerates depended on the temperature at which agglomeration was triggered and on the ligand chain length. For a given ligand chain length N_c, crystalline agglomerates were only observed above a specific "crystallization temperature" T_c.

amorphous agglomerates like the one shown in the inset of Fig. 1.

When we added poor, polar solvent, DLS indicated agglomeration at much higher T_p, as expected. T_p in polar solvents was often so high that we could not sufficiently heat the solvent to dissolve the agglomerates. We precipitated agglomerates at different temperatures by adding polar solvent, removed the agglomerates from the solution, and prepared them for TEM observation.

Although all samples were prepared for TEM identically, there were clear morphological differences depending on temperature: agglomerates formed in polar solvent below a ligand-dependent "crystallization temperature" T_c were consistently amorphous (see Fig. 2), whereas agglomerates formed at temperatures above T_c contained crystalline arrangements of nanoparticles. Crystallinity was clearly visible in electron transmission and diffraction. We also recorded synchrotron small-angle x-ray scattering (SAXS) spectra of the agglomerates in solvent and found the same temperature-dependant crystallinity (see the Supplemental Material [15]).

The crystallization temperature T_c increased with the ligand chain length similarly to the agglomeration temperature T_p. Crystallization occurred above $-7\,^{\circ}\mathrm{C}$ for C12, above $42\,^{\circ}\mathrm{C}$ for C16, and above $52\,^{\circ}\mathrm{C}$ for C18 particles, respectively. These temperatures correlate to reported melting temperatures of particle ligand shells of approximately $-5\,^{\circ}\mathrm{C}$ (C12), $40\,^{\circ}\mathrm{C}$ (C16), and $50\,^{\circ}\mathrm{C}$ (C18) [16]. Differential scanning calorimetry experiments confirmed that our particles' ligand shells melt at around T_c.

Our observations are summarized in an N_c-T phase diagram (Fig. 3) with two phase boundaries: the transition from dispersed to agglomerated particles at T_p upon cooling in good, unpolar solvent and the transition from amorphous to crystalline agglomeration at T_c in poor, polar solvent. Two features of this phase diagram are unexpected. First, agglomeration occurs at higher temperatures for particles with longer ligand chains. One would expect longer chains to shield the dispersive attractions between the gold cores better, lower the energy difference between the dispersed and agglomerated state and, therefore, lower the agglomeration temperature. Second, crystalline agglomerates occur only at high temperatures.

The lowest energy state of spherical monodisperse particles is crystalline [17]. Amorphous configurations can be stabilized by size polydispersity [18], anisotropic interactions [19], or jamming of the particles [20]. We can rule out size polydispersity as an origin for this behavior because the same samples exhibited amorphous packing at low temperatures and crystalline ordering at higher temperatures. The interactions between the gold cores are unaffected by temperature in the ranges of our experiments. Instead, we believe that amorphous agglomeration is governed by the contact mechanics of the ligand shells.

Because neither analytical theories nor energy-based Monte Carlo simulations can describe the velocity-dependent dynamics of the interacting viscous ligand layers, we used Langevin dynamics simulations [21,22] to investigate the experimentally observed behavior. Nanoparticles with alkyl thiol coatings were modeled as spherical beads with a Hamaker type attraction between the gold cores and a suspension stabilizing repulsion from

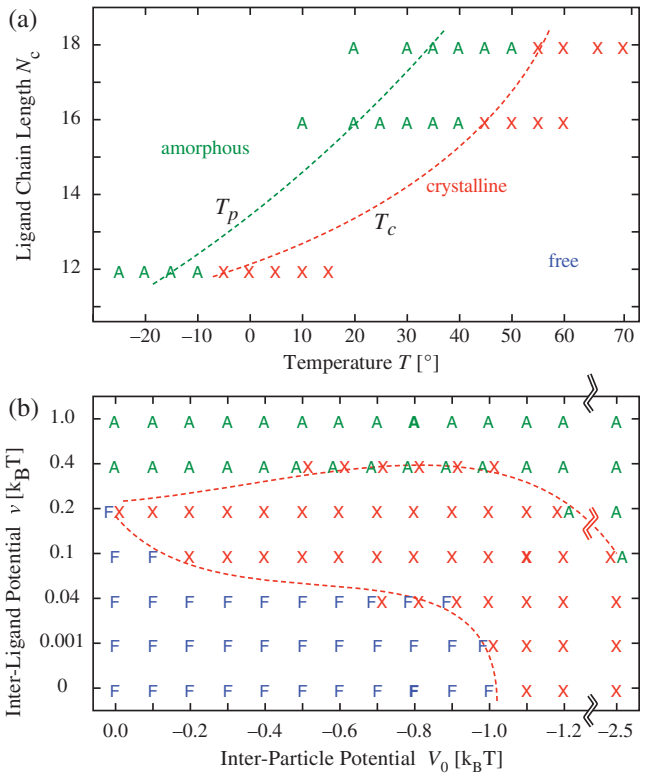

FIG. 3 (color). Agglomeration behavior from experiment and simulations. The letters A, X, and F denote amorphous, crystalline, and free agglomerates, respectively. (a) Experimentally determined phase diagram for the formation of amorphous and crystalline agglomerates. N_c denotes the number of carbon atoms in the ligand chains on the particles. The red line visualizes the boundary T_c between precipitation of crystalline and amorphous agglomerates in poor, polar solvent and the green line the onset of agglomeration at T_p upon cooling in good, unpolar solvent. (b) Phase diagram from simulations showing the agglomerates' morphology depending on the radial interparticle potential V_0 and the transient interligand stiction barrier height ν. The broken red lines are guides to the eyes to visually distinguish the three regimes more clearly.

the overlap of the ligand shells. We first tested whether the viscosity of the ligand shells could explain amorphous agglomerates. For this, the viscosity of the alkyl thiol shells was phenomenologically represented by additional hydrodynamic interactions [23]. However, regardless of the choice of parameters we found either free nanobeads or crystalline agglomerates as stable states. Agglomeration was slowed down by this ligand viscosity, but this velocity-dependent interaction could not stabilize the amorphous agglomerates.

Correct modeling of the alkyl thiol monolayers that form the ligand shells of our particles apparently requires a more complex model. The monolayers are known to exhibit a phase transition between a molten and an ordered solid state, with the respective melting temperature close to the amorphous-crystalline transition temperature T_c observed in our experiments [16]. Rather than setting up a detailed model of the many flexible alkyl thiol chains, we used a phenomenological description akin to the classical model of stiction. Typical relaxation times of polymers are on the order of 10^{-7} s, while a Brownian collision between particles occurs on a scale of around 10^{-1} s [14]. The dynamics of the ligand chains are therefore neglected in the model. Instead, spontaneous harmonic bonds are established within overlapping regions of the ligand shells of adjacent beads. These elastic contacts can be broken when they are strained beyond a certain tension [see Figs. 4(a) and 4(b)]. The two central parameters are the depth of the radially symmetric interparticle potential, V_0, and the barrier height ν of the transient sticky interligand potential. The case of nonsticky particles is recovered for $\nu \to 0$. Further details on this model can be found in the Supplemental Material [15]. We expect that the particles will form crystals for $\nu \to 0$ and $V_0 < -1k_BT$, but that a sufficiently strong transient interligand potential ν will cause the particles to stick together wherever they first touch so that they remain trapped in amorphous agglomerates.

The simulations were run with 100 beads in a 100 nm wide cubic simulation box with periodic boundary conditions. To classify the ordering of the agglomerates, a distance cutoff was used to convert the snapshots into an association network [22,24], from which the degree distribution $P(k)$ was determined and then averaged over the runs and over time. Typical $P(k)$ curves are shown in Fig. 4(c). For unbound beads, the "neighbors" result from

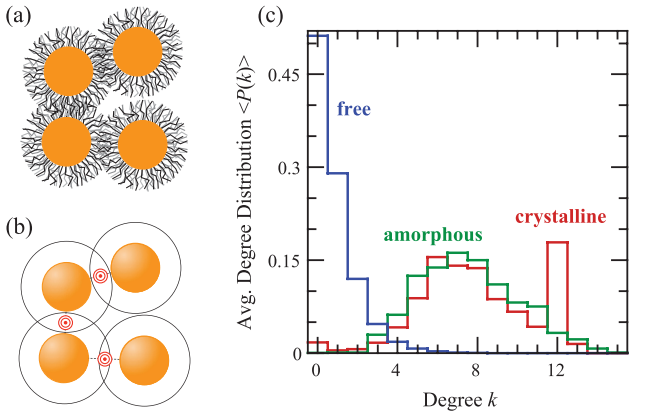

FIG. 4 (color). Implementation of the transient interligand potential. (a) Sketch of four nanobeads forming a complex in which the ligand shells partly overlap and the ligands on different beads interdigitate. (b) In the simulations, transient interligand "bonds" phenomenologically describe how the ligands from different nanobeads stick to each other. These bonds break when the two nanobeads are displaced or rotated relative to each other by more than a specified distance. (c) Typical averaged degree distributions obtained from the particle association networks from the simulations for the cases of free particles (blue) and for amorphous (green) and crystalline agglomerates (red), respectively.

transient collisions with other beads. The maximum of $P(k)$ is at $k = 0$. There were rarely more than four beads touching in any of the snapshots [blue curve in Fig. 4(c)]. For an amorphous aggregate, $P(k)$ has a broad maximum around $k = 6 \ldots 8$ (green curve), while a hexagonal crystal lattice is characterized by a distinct peak at $k = 12$ direct neighbors. For an infinite perfect lattice this peak would be the only nonzero value of $P(k)$, but in our simulations many beads reside on the surface of the small crystallite. This leads to the shown broad distribution around $k = 6 \ldots 8$ plus the distinct $k = 12$ "crystal peak" (red curve).

Scanning V_0 and ν, we obtained the phase diagram shown in Fig. 3(b). As expected, the beads did not agglomerate for small values of both V_0 and ν. Strong interligand potentials ν led to amorphous aggregates regardless of the interparticle potential V_0. Between these two regimes, crystalline agglomerates formed for vanishing ν and $V_0 < -1 k_B T$—attractive particles with a smooth surface—and for ν between $0.04 \ldots 0.4 k_B T$ in a wide range of V_0, i.e., for weakly attractive particles with some ligand stiction. For $V_0 \to 0$ the crystalline region narrowed, but ordering was found even close to $V_0 = 0$.

Interestingly, crystalline agglomerates formed for weakly attractive cores (small V_0) with interligand potentials well below the usual threshold of $1 k_B T$. Here, agglomeration is a multiparticle process where an incoming bead touches multiple other beads. Together they can prevent it from leaving again while it can still move to an energetically more favorable position. Only when the interligand binding became too stiff for $\nu > 0.4 k_B T$ was rearrangement hindered and were amorphous complexes formed.

For an interpretation of the experimental findings we now have to map the three variables of the experiments, the temperature T, the ligand chain length N_c, and the solvent polarity, to the two simulation parameters V_0 and ν. First, consider agglomeration above T_p induced by a more polar solvent. This corresponds to an increase of the spherical interparticle attraction V_0 below $-1 k_B T$ in the simulations which leads to agglomeration regardless of the ligand interaction. Second, when T is increased in the experiments, crystalline rather than amorphous agglomerates are found. This transition occurs in the simulations when the spontaneous interligand potential ν is decreased. The opposite transition is observed in the experiments for an increasing ligand chain length N_c; i.e., an increase of N_c corresponds to a deeper ν.

Two experimental variables—N_c and T—therefore define the simulations' ν, but with opposite effects. To keep ν constant for longer chains, T has to be increased. The experimental phase diagram highlights this balance: the longer the ligands, the higher the transition temperature between amorphous and crystalline agglomeration. The diagonal boundary in the experimental T-N_c phase diagram that separates crystalline from amorphous agglomerates therefore corresponds to an approximately constant ν in the simulation. A graphical representation of this mapping is a clockwise rotation of the experimental T-N_c phase diagram by roughly 45°.

Thus, spontaneous entanglement of the ligand shells is required in the simulations to reproduce the experimentally observed behavior. A spherically symmetric interparticle potential alone is insufficient to explain the observed order-disorder transition. Both the interparticle and the interligand potentials contribute to the energetic landscape in which agglomeration takes place. The spherically symmetric interparticle potential defines the global minimum, i.e., the crystal state, while the spontaneous ligand-ligand contributions provide local energy barriers that can keep the agglomerate in a metastable amorphous state.

These local energy barriers also explain why the agglomerates are more stable at higher temperatures when the alkyl ligand chains are longer: the stronger spontaneous entanglement between the thicker ligand shells more than compensates for the reduced core-core attraction due to the larger separation. Furthermore, the addition of a polar solvent reduces the solubility of the ligand shells such that not only the gold cores but also the ligands contribute to the isotropic attractive interparticle potential.

The importance of the ligand-ligand interactions for the agglomeration process is remarkable. Gold has a large Hamaker constant and alkyl thiol monolayers are amongst the thinnest ligand shells used in unpolar particle dispersions. We may therefore conclude that the assembly of nanoparticles with lower Hamaker constants that do not involve permanent charges or dipoles is dominated by the ligand shells, too. Even the attractive contribution that causes agglomeration may be due to the ligands. We note that such a small influence of the core-core interaction on nanoparticle assemblies is consistent with results by Luedtke and Landman who performed molecular dynamics simulations on small alkyl thiol passivated gold nanoparticles in vacuum [25].

These results have profound consequences for the understanding and application of particle-based materials. So far, ligands have mainly been chosen for synthetic convenience and to provide a stable dispersion. We show here that the interactions upon contact (measurable, for example, by colloidal AFM [26]) are important factors in particle assembly. A careful choice of ligands increases the propensity of the particles to self-assemble. We believe that further tuning of the contact mechanics between particles will allow us to target a wide range of agglomerate structures in a single colloid: loose, fractal diffusion-limited aggregation structures, amorphous agglomerates, and dense, crystalline particle superlattices can all be formed on demand.

P. B. and T. K. thank Eduard Arzt for his continuing support of the project. We acknowledge beam time at HASYLAB's BW4 small-angle scattering beam line and the support of Jan Perlich. Funding from the German

Science Foundation DFG is gratefully acknowledged. T. Geyer and P. Born contributed equally to this work.

*tobias.kraus@inm-gmbh.de

[1] L. Vayssié, F. Skouri, L. Sperling, and J. Cohen, Biochimie **82**, 269 (2000).
[2] C. B. Murray, C. R. Kagan, and M. G. Bawendi, Annu. Rev. Mater. Sci. **30**, 545 (2000).
[3] M.-P. Pileni, Acc. Chem. Res. **40**, 685 (2007).
[4] D. V. Talapin, J.-S. Lee, M. V. Kovalenko, and E. Shevchenko, Chem. Rev. **110**, 389 (2010).
[5] H. Verduin and J. K. G. Dhont, J. Colloid Interface Sci. **172**, 425 (1995).
[6] S. Roke, O. Berg, J. Buitenhuis, A. van Blaaderen, and M. Bonn, Proc. Natl. Acad. Sci. U.S.A. **103**, 13310 (2006).
[7] A. P. R. Eberle, N. J. Wagner, B. Akgun, and S. K. Satija, Langmuir **26**, 3003 (2010).
[8] M. Sztucki, T. Narayanan, G. Belina, A. Moussaid, F. Pignon, and H. Hoekstra, Phys. Rev. E **74**, 051504 (2006).
[9] D. V. Talapin, E. V. Shevchenko, A. Kornowski, N. Gaponik, M. Haase, A. L. Rogach, and H. Weller, Adv. Mater. **13**, 1868 (2001).
[10] M. B. Sigman, A. E. Saunders, and B. A. Korgel, Langmuir **20**, 978 (2004).
[11] M. Y. Lin, H. M. Lindsay, D. A. Weitz, R. C. Ball, R. Klein, and P. Meakin, Nature (London) **339**, 360 (1989).
[12] N. M. Dixit and C. F. Zukoski, Phys. Rev. E **67**, 061501 (2003).
[13] N. Zheng, J. Fan, and G. D. Stucky, J. Am. Chem. Soc. **128**, 6550 (2006).
[14] F. T. Hesselink, A. Vrij, and J. T. G. Overbeek, J. Phys. Chem. **75**, 2094 (1971).
[15] See Supplemental Material at http://link.aps.org/supplemental/10.1103/PhysRevLett.109.128302 for details on the particle and agglomerate characterization to support our interpretation of the TEM studies, a comparison to SAXS results, and further details on the simulation model and the software used.
[16] A. Badia, S. Singh, L. Demers, L. Cuccia, G. R. Brown, and R. B. Lennox, Chem. Eur. J. **2**, 359 (1996).
[17] C. Valeriani, E. Sanz, P. N. Pusey, W. C. K. Poon, M. E. Cates, and E. Zaccarelli, Soft Matter **8**, 4960 (2012).
[18] M. Fasolo and P. Sollich, Phys. Rev. Lett. **91**, 068301 (2003).
[19] J. P. K. Doye, A. A. Louis, I.-C. Lin, L. R. Allen, E. G. Noya, A. W. Wilber, H. C. Kok, and R. Lyus, Phys. Chem. Chem. Phys. **9**, 2197 (2007).
[20] P. N. Pusey and W. van Megen, Nature (London) **320**, 340 (1986).
[21] U. Winter and T. Geyer, J. Chem. Phys. **131**, 104102 (2009).
[22] T. Geyer, BMC Biophys. **4**, 7 (2011).
[23] T. Geyer and U. Winter, J. Chem. Phys. **130**, 114905 (2009).
[24] F. Lauck, V. Helms, and T. Geyer, J. Chem. Theory Comput. **5**, 641 (2009).
[25] W. D. Luedtke and U. Landman, J. Phys. Chem. **100**, 13323 (1996).
[26] M. Kappl and H.-J. Butt, Part. Part. Syst. Charact. **19**, 129 (2002).